Link to Publisher's version: ***http://dx.doi.org/10.1016/j.ecss.2016.08.011***

Citation: Itugha OD, Chen D and Guo Y (2016) Pollutant advective spreading in beach sand exposed to high-energy tides. Estuarine, Coastal and Shelf Science. 181: 70-82.

Pollutant Advective Spreading in Beach Sand Exposed to High-Energy Tides

Okuroghoboye D. Itugha[1], Daoyi Chen[2] and Yakun Guo[3]

ABSTRACT

This paper presents field measurements in which dye solute was injected into coastal sand to investigate contaminant advection in intertidal beach sand. The measurements show the pathways of a contaminated plume in the unsaturated zone during both the flood and ebb tides. A prescribed amount of dye tracer solution was directly injected through the topsoil, with average porosity 0.3521±0.01, at predetermined locations of the River Mersey's outer estuarial beach during ebb-tide. The injected dye was monitored, sampled and photographed over several tidal cycles. The distinctive features of the plume (full two dimensional cross-sections), sediments and water-table depth were sampled in-situ, close to the injection point (differing from previous contaminant monitoring tests in aquifers). The advective movement is attributed to tidal impact which is different from contaminant transport in aquifers. The experimental results show that plumes have significantly large spatial variability, diverging upwards and converging downwards, with a conical geometric shape which is different from the usual spherical/elliptical shape reported in literature. The mean vertical motion of the plume reaches three times the top-width within ten tidal cycles, exceeding the narrow bottom-width by a factor of order 2. The observed transport features of the plume within the beach sand have significant relevance to saltwater intrusion, surface water and groundwater quality. The field observations are unique and can serve as a valuable benchmark database for relevant numerical studies.

Keywords: *Coastal foreshore, dye migration, River Mersey Estuary (RME), interstitial hydraulics, groundwater table.*

[1]Faculty of Engineering and Technology, Civil & Environmental Engineering Department, Federal University Otuoke, 400 University Boulevard, Otuoke, PMB 126, Bayelsa State, Nigeria. Email: itughaod@fuotuoke.edu.ng

[2]Ocean Science and Technology Division, Graduate School at Shenzhen, Tsinghua University, Shenzhen 518055, P.R. China. **Corresponding Author Email:** chen.daoyi@sz.tsinghua.edu.cn

[3] School of Engineering, University of Bradford, BD7 1DP, UK. Email: y.guo16@bradford.ac.uk

1 INTRODUCTION

Most contaminated beach sediments near industrial cities in Europe show relatively high concentrations of heavy metals and persistent organic pollutants (POPs) even though many years have passed since they were firstly polluted. This seems to be the case with estuaries whose watercourses pass through urban and highly industrialised areas, even after the surface water has been treated. This poses threats to the ecosystem and biodiversity due to releases associated to toxic sewage, and to remediation efforts often neglecting the river bed.

In the United Kingdom a number of estuaries, such as the Thames, the Mersey, and the Humber, have had well documented accumulation of untreated domestic and industrial sewage. One special case is the River Mersey Estuary (RME, in north-west England), which is connected to Liverpool Bay at the Outer Estuary (see Fig 1). It directly exchanges tidal input and output with the Irish Sea through Liverpool Bay, where the sands vary from medium to fine. The catchment area of the RME is densely populated and highly industrialized, and the RME is described as one of the most polluted water ways in Europe with flow rates promoting high turbidities (Turner et al, 2002; King et al, 2004; Jones, 2006). It has been reported that a large concentration of contaminants still persists in extensive RME and Liverpool Bay intertidal beach sediments. For example, concentrations of Mercury (Hg), caused by use of Castner-Kellner processes, remain as high as 2 mg/kg at discharge outlets linked to chemical plants in the Widnes–Runcorn areas of RME (Fox et al, 1999; Vane et al, 2007). [Mercury is associated with organic matter and is toxic to marine invertebrates with potential effects on humans through ingestion of fish and shellfish]. However, the toxicity levels in the sediments tend to decrease in the Liverpool Bay regions away from the discharge outlets (Rogers, 2002). Burt et al (1992) reported the upper and lowest mean levels of Hg in the sediments as 1.2 and 0.01 mg/kg (in 40% silt), respectively. POPs, polyaromatic hydrocarbon (PAHs) and polychlorinated bipheniles (PCBs), in the sediments of RME, its tributaries and Manchester Ship Canal, may have originated from oil refineries, sewage, paper and chemical works, dockyards, power stations and shipping activities (Jones, 2006). King et al (2004) found that PAH levels in the sediments were much more concentrated at depths of 0.5-0.53m. PCB concentration in the RME is believed to be higher than that in the Thames and the Humber estuaries. Recent observations by Vane et al (2007) show no declining trends of PCBs but implied that the Outer Estuary areas are 30 times less contaminated than the Inner Estuary. To our best knowledge, no clear relationship between contaminant movement and tidally mediated fluxes in beach sediments has been reported so far. However, Rogers et al (1992) suggested that the presence of these substances deep in the RME sediments may have been due to tidally induced diffusive mixing.

Organic matter content between sandy (low organic content) and marsh sediments can also strongly affect PAH concentration distribution (King et al, 2004). Huang et al (2003) identified that hydrophobic organic contaminants (HOCs) can readily mix in benthic organic sediment (BOS) environments. They identified the importance of understanding and quantifying varied HOC properties for the prediction of transport and eventual fate in aquatic environments.

The vadose zone (intermediary between seawater and groundwater) of the RME intertidal beach is affected by very complex hydrological processes from high-energy semidiurnal tides. The beach water table rises and falls with the sea level. So water-borne sewage or sewage discharged from urban, coastal recreational and industrial activities can enter and be retained or redistributed (Diaw et al, 2001). Martino et al (2002) suggested that trace-metals accumulated in beach sediments could be released by kinetic (advective) re-suspension processes and desorbed to the overlying watercourse. Accurate field studies/measurements are limited due to the complex hydrological environment as the parameters controlling convective activity in-situ become more difficult to quantify (Wexler, 1992; Zhang et al, 2002; Precht and Huettel, 2004). As a result, there is presently poor understanding of the movement and spreading of anthropogenic substances (such as land-applied chemicals), spills and leaks that eventually enter beach sediments and consequently the freshwater domain (Mao et al, 2006). This may partly explain that considerably more research is conducted on contaminant transport in coastal groundwater (GW) aquifers than on transport in beach sediments (Lanyon et al, 1982; Diaw et al, 2001; Mao et al, 2006; Denham and Vangelas, 2008). More studies on groundwater behavior in sandy beaches, with relationships between tide and water-table, can be found in Baird and Horn (1996); Turner and Leatherman (1997); Kalbus et al (2006); and Berkowitz et al (2008).

Pressure fluctuations can have a significant impact on interstitial oxygenation processes, thus on fates of contaminants and in some cases on aquatic life (McLachlan, 1989; Precht and Huettel, 2004). Water movement is routed via complex pores and varies with depth and degree of compaction. The properties of the sand (porosity ϕ, grain size and grading) and the dye (density ρ, and dynamic viscosity μ) are therefore important to determine the role of hydraulic conductivity (Fetter 1999). This is because the local unsaturated hydraulic conductivity depends on the degree of soil - water content and/or pressure head (Mohanty et al. 1994; Gupta et al. 1993). Typical porosity for medium to fine sand ranges from 26% to 53% (Domenico and Schwartz, 1997). Barnes (1995) estimated the hydraulic conductivity values of sand and sand-gravel mixtures to vary significantly from 0.036m/hr to 36m/hr respectively. Fox et al (1999) showed that the sediment cores of the RME (e.g., Widnes – Runcorn areas) are made up of 2-5% sand with size distribution of 63-2000μm, 70-75% silt (2-63μm), and 25-27% clay (<2μm).

The use of conservative tracers to simulate contaminant movement in the field is a known robust technique. However, Robbins (1989), Callaghan and Codd (1998) and Precht and Huettel (2004) have shown that use of tracer monitoring devices in intertidal beach sand may not provide reliable qualitative and quantitative concentration data. This is because the intrusive techniques, such as probes and positron emission tomography, can affect the natural flow regime in the subsurface environment.

This study was motivated to attract attention of remediation efforts to consider flushing of the river bed sediments and foreshore (water quality management issues), along with treatment of the surface water in estuarine areas of this nature. It reveals that tides can induce surface water – vadose zone - groundwater interactive transport. The study was also motivated by the fact that most methods for monitoring the contaminant in the field involved intrusive techniques, such as probes and positron emission tomography, which are known to affect the natural flow regime in the subsurface environment, hence may not present the expected natural phenomenon. Therefore, there is a need to visualize full shapes of the plume in the field in order to investigate the contaminant movement in beach.

2 SITE CONDITION AND METHODOLOGY

A non-intrusive method is employed is employed to investigate the contaminant movement in beach sand subject to large tidal range in this study. A conservative tracer (dye) is injected 0.05m below the unsaturated beach sediment surface. The experiments lasted over one to ten semidiurnal tidal cycles during the summer months of 2006 and 2007. Sediment characteristics, water table depth of the intertidal zone and the spatial variability of fully extracted plumes were sampled, processed and analyzed.

2.1 Study area

The experiments were carried out in Liverpool Bay (the RME Outer Estuary injection site (OEIS) and Narrows (Narrows Estuary injection site (NEIS); 53′26″N and 03′02″W) at New Brighton, England (see Fig 1). The Mersey Estuary of Northwest England has an area of approximately 5000 km^2, with a history as one of the most polluted estuaries in Europe (WPRL, 1974; Jones, 2000; Vane et al, 2007). Its catchment has a high density of population up to 5 million, including the major municipalities of Liverpool and Manchester, and was heavily industrialized. RME consists of four divisions, namely the Upper, the Inner, the Narrows and the Outer Estuary.

The Outer Estuary includes a large intertidal sand beach, with a range of facilities at the sheltered corner of the coast and a marine lake seawards of the shoreline. The Narrows is an ostrich-neck-like convergence with breadth measuring 1.0-1.5 km and a maximum depth of 30 m. The broader Inner Estuary is a characteristic mixed estuary with salinity measuring an equivalent of 4g/l at low tides to 11g/l at high tides. The current passing through the Narrows has a velocity up to 2m/s at spring tides.

Generally speaking, tides from the Irish Sea directly enter the RME during the flood phase through Liverpool Bay and discharge to the Irish Sea during the ebb phase. Tidal range is between 10.7m (maximum springs) and 4.0m (minimum neaps). The water volume of the RME varies from 0.7 x 10^7 m^3 at low tide to 3.5 x 10^8 m^3 at high tide, indicating a significant effect on the catchment. The mean sea level (MSL) is about 5.214m above the ordinance datum (AOD) (Admiralty Tide Tables, 2005). The strong tidal currents sustain large sandbank build-up in the estuary. The sheltered boundary may be affected through groundwater flow from the wave run-up and infiltration at the intertidal reach.

The exposed beach consists of a variation of medium to fine sand and localized mud banks. The aquifers of sheltered and of intertidal boundaries receive water from the prevailing tidal regime. There are several borehole wells that litter the sheltered boundary, the closest of which to any of the injection sites is about 1km. The Marine Lake however is less than 20.0m from OEIS-IZ (A) and has depth varying from 5.0m at the west end to about 0.5m at the east end. The intertidal zone of OEIS from the inland beach bank to the shoreline at low ebbs averages between 345m and 450m. At the NEIS area, the width of the intertidal zone varies from about 45m to 368m.

2.2 Experimental design, material and method

2.2.1 Site preparation, tracer type and dye injection

Tests were carried out at three OEIS injection zones (IZs), namely A, B, and C, and two NEIS injection zones, namely A and B. The activities on site included surveillance and delineation of the site, dye injection, sampling, plume measurement, core sample collection, GPS location and elevation recording. Each IZ defines multiple sampling points (SPs, see Table 1 which lists the total injected points and the sampled injected points.) with two rectangular dimensions of 1.5 x 2.5 m^2 and 2.5 x 2.5 m^2 on the unsaturated beach surface. Dye injection was not repeated on any previously used SP to avoid the effect associated with disturbed flow field resulted from previous injection and sampling activities. The SPs were not equally spaced apart but separated by a distance of at least 5.0m as measured by a 15.0m fiberglass tape. The rectangular arrays were divided into 0.5 (length, l) x 0.5 (breadth, b) m^2 square cells so that each SP consists of 15 or 25 injection points (IPs) in 3x5 or 5x5 column/row grids (arrays) respectively (see Fig 2 and Table 1). This means that the injected dye was entrapped within a volume of 0.13125 m^3 (*l*=0.5) x (*b*=0.5) x (depth *h*=0.525). The locations of SPs were recorded using a 12-channel Garmin GPS 76 marine navigator with precision of about ±2m. The inject dye was a red color 810 (E124) conservative agent with 4.3% pure dye content, and density of 0.947g/cm^3 - 1.022g/cm^3. Since the solution is conservative food dye, it is expected that it is not absorbed to the sand surface.

2.2.2 Tracer solution injection and monitoring

The dye solution (5.0ml portion) was injected at 0.05m below the beach surface (about 1.55m below the high tide mark) during low water. The choice of 0.05 m injection depth is considered to be reasonable since the first 0.05m coastal sand region readily stimulates oxygen injection and utilization into deeper layers (Rusch et al 2000; Ehrenhauss and Huettel 2004). A 10.0ml Pressure-Lok precision sampling purge and trap syringe system with appropriately calibrated hypodermic needles of size 0.028″ x 0.012″ x 2″ was used to inject the dye. Fig 3 demonstrates that the sampling zone (area) at OEIS-IZ(A & B) generally varies between about 75 to 185m offshore from the inland beach back barriers. The vertical line of injection (needle-line) is as thin as the natural soil pores hence assumed non-intrusive. The amount of solution injected and the depth of injection remained the same in the experiments. Field activities were repeated through three months during the summer (17/April-17/July 2006; 2007), always at neap tides. Though winter tests were carried out for three months (22/November 2005-19/January 2006) at OEIS-IZ(A), the success rate was low due to harsh field conditions. The atmospheric environment during the experiments was not only under sub-zero temperatures but also very windy during November 2005 to January 2006. As such, it was not convenient (health/safety and clarity-wise) to conduct sampling/measurement/recording activities in the field, meanwhile to ensure the measurement accuracy. Therefore, only the summer samples at OEIS-IZ (A and B) are reported here. The injected sample was monitored through several tidal cycles (1/4, 1, 2, 4, 6, 8, 10, 12, and 14). The injection always took place at the start of the low tide, therefore, there is no difference of start state of tide and the state of tide effect on the spread of dye is the same.

2.2.3 Tracer plume sampling, measurement and parameterization

On detecting the contaminated surface area (*l* x *b*), each boundary was carefully sectioned using hand trowels to penetrate the undisturbed plume domain. The volume (*l* x *b* x *h*) of the sand from the surface was sliced from the edge towards the center of the square (*l* x *b*). This was done on each occasion to maximize recovery and measurement of the full 2D plume shape (see Fig 4).

The geometry of the plume was measured from the photograph taken using a Nikon Coolpix 8800 digital camera of 8.0 effective megapixels. Figures 4a, b and c are the photos taken at various times indicated in figure caption after injection. It shows the vertical extent of plume, depth of plume center and the top and bottom widths of plume at various elapse times of injection. Figure 5 demonstrates and summarizes these parameters. A Cartesian coordinate system is established using the horizontal line passing the injection point as the x-axis and a vertical line some distance away from the plume center line as the y-axis.

As the vertical advective spreading is a cone shape, a trapezoidal shape is adopted (see Fig 5) to evaluate the plume. The top and bottom (front) width of the plume are defined as W_1 and W_2 respectively. The infiltration depth is the vadose zone with horizontally infinite dimensions. The depth GI is the depth of injection at I = (0.25,-0.05) while GH represents Y_0, the depth of the center of mass of the cone (Fig 5; Y is the (vertical) depth coordinate).

2.2.4 Depth-to-water and water-table elevation measurement

Water table elevation (WTE) at OEIS-IZ (A and B) and NEIS-IZ (A) was determined by measuring the depth-to-water table (DTW) and beach surface elevation using a GPSMAP 62S which has 5ft – 12ft margin of error. DTW was taken as the depth below the beach surface to the top of the saturated material (subtidal), where the mean pore pressure is atmospheric (zero) (Nielsen, 1997). The elevation and shape of the water table surface respond to surface water features resulting from recharge and discharge changes. The DTW measurements averaged to about 0.525m, which is relevant towards the depth of IP in relation to the high tide mark (HTM, see Fig 3). Fig 6 is a typical example showing the variations of the mean elevations of the beach surface and the depth to water table with beach width. The water-level data were converted from depth below surface to WTE using the beach surface elevation (BSE) measured by GPS. In Fig 7, the Kozeny-Carman relation (Klute and Dirksen, 1986) is applied to show the permeability of core samples taken from injection sites with different grain-sizes. Fig. 8 shows the influence of tidal variation on the water level of the closest borehole well to the OEIS-IZ and NEIS-IZ, and marine lake water levels at the sheltered coast.

3 RESULTS AND DISCUSSIONS

3.1 Physical properties of beach sediment

The grain-size distribution of the cores (Samples A-F) showed 96.3 to 100% sand (medium to fines), 1.3-3.4% silt, 0.1-0.3% clay and 1.4-3.7% mud. The median grain size (d_{50}) is spatially variable ranging between 0.196m and 0.259m, while the geometric mean of lognormal distribution of the diameter varied from 0.176mm to 0.258mm. The effective grain-size (d_{10}) also varied between 0.121mm and 0.188mm. The ratio of geometric mean grain size to median grain-size varied from 0.901 to 0.996, with particle standard deviation varying between 1.266 and 1.966. The porosity of the sand determined in the laboratory using the volume of voids to total volume was 0.352 with confidence level of ±0.01. The coefficient of uniformity Cu was 1.531±0.08 (95% confidence intervals) < 4. The coefficient of curvature Cc, which is dependent on factors of shape and symmetry, was 0.287±0.01 (95% confidence intervals). Values of Cu between 1 and 3 normally define well-graded sediment materials. The value of Cu here shows that size is reasonably regular, hence high porosity and vulnerability.

The optimal moisture content in the capillary fringe above the water table at the maximum density of 1309.4kg/m^3 was determined as 20.5% using the first 15cm of unsaturated core samples from OEIS. The specific yield varied between 0.176±0.004 and 0.214±0.02 using the untreated core specimens. Averaged permeability K of the sampled sand at OEIS-IZ (A & B) and NEIS-IZ(A) was determined to be 1.482×10^{-5} m/s using the method of the Falling-head (Klute and Dirksen, 1986).

Fig 7 is the comparison of permeability of the cores for the sites using the Kozeny-Carman relation, which is adopted because it incorporates grain-size distribution and shape (Carrier 2003). Fig 7 shows that the permeability of the investigated intertidal sediments decreases with the increasing of the sand percentage passing the sieve size. Larger difference of the permeability of sediments at various sites is found for the lower sand percentage passing the sieve size while this difference decreases for higher sand percentage of passing the sieve size. More pressure is needed to squeeze the injectate through sediment with low permeability (i.e. high sand percent passing) than in zones with high permeability (i.e., low sand percent passing). The grain-size distribution of the cores in this study showing high sand percent passing is mainly from medium to fine sand. It is also seen that the permeability of the intertidal sediments at the OEIS-IZ (A) was much higher than that of others at the lower sand percentage passing the sieve size. However, the permeability of sand at the OEIS-IZ (A) decreases sharply with the increasing of sand percentage passing the sieve size and is lower than that of sediments taken in other sites. The results are in good agreement with published data in literature for the same category of marine sand (Todd, 1980; Mason, 1997; Li et al, 2009). In-situ values of permeability are usually larger than laboratory estimates as shown in Li et al (2009), so the values of K found in this study are at the lower end.

3.2 Influence on local groundwater (GW) table by tidal events

Monthly-averaged Liverpool sea level from the records at the British Oceanographic Data Centre (BODC) was5.154m in August 1991 and rose to 5.177m in December 2006 while the annual mean of 1991 was 5.158m and by 2006 it was 5.401m. Woodworth et al (1999) showed in an earlier study of data covering the period of 1858 to 1998 from all three (3) tidal water stage markers (Gladstone, Alfred, and Princes Pier) that the mean sea levels had a relative increase of 0.17m. The tides at Liverpool are predominantly semi-diurnal with mean tidal range of 6.7m (Woodworth, P. L. and Blackman, D. L. (2002)). The maximum high water and the minimum low water sea levels observed during this period were recorded as 10.821m and -0.181m on 10/02/1997 at 1244hrs and 20/02/1996 at 1915hrs respectively. Fig 8 shows the effect of the change of water head at the seaward boundary on the coastal barrier aquifers in 2006. The rise and fall in the data shows that the local groundwater system may be connected or influenced by tidal events.

The marine lake water levels were averaged between 2006 and 2007 for different (west to east) locations. The highest water level in the lake was recorded at the western end.

3.3 Depth of advection and spreading scenario of contaminant in beach sand

To investigate the advection and spreading of plumes, dimensions averaged for the sites in Fig 5 will be used to plot the movement of plumes in space with time.

3.3.1 Scenario at OEIS-IZ (A) – summer

A ‘no-flood’ case was initially tested by injecting the conservative dye through the unsaturated beach surface and waiting for about 5 hours. The well water level variations were taken from a relatively distant borehole-well (sj39/130). A second test was an extension to one complete tidal cycle where dye was injected while the beach surface was unsaturated and then waiting through one full saturation-unsaturation cycle. About 50 samples were collected at different locations and Fig 4a, b and c shows the comparison of the output from some of the tests. In Fig 4a, the dye was allowed for up to 5 hours in the sediments with no tidal flooding on the beach. All the plume pools in this case look identically circular or spherical in shape when sampled. The mean cross-sectional area was within a 95% confidence interval of $3.384 \times 10^{-3} \pm 2.6 \times 10^{-4} m^2$. This type of response was attributed to convective flow since there was no visible recharge that initiated the spread. Again, when the dye was monitored through one complete tidal (saturation-unsaturation) cycle, the plume pools changed to conical shapes covering an averaged area of about $0.0032 \pm 0.001 m^2$ within the entrapment volume (l x b x h). A further change evolved in the conical contour when the monitoring period was increased to two complete tidal cycles (Fig 4c).

The area of these plumes was a similar order of magnitude as in the one-cycle case. Without field observations, intuition for plumes in a porous medium would suggest either a spherical or elliptical shape. Conical shapes of this nature have not been reported in literature, at least not to the authors' knowledge. The determination of the magnitude of the plume and shape could help towards understanding the extent of dye concentration, direction of distribution and eventual fate in intertidal coastal zones with similar properties. The formation of plumes as shown in Figs 9 (Top and Bottom) demonstrates the effect of pressure variation in the vadose zone. It is seen from Figs 9 (Top and Bottom) that the inclination of the tidally induced plumes highlights the processes of horizontal mass transport and pressure gradient variation controlling coastal groundwater table fluctuation. Fig 9 (Top) shows a collection of samples representing the general behavior of the injective in OEIS-IZ (A**)** from day-1 to day-5. It shows the progressive formation of a plume by advective spreading in space with time. With infiltration, the pressure in the pore medium decreases as zones of low pressure is created in the area of the IP. The progression of subsidence affecting the plume in space with time can be observed clearly. The H_p (height of plume-top below injection-position) varies from 0.09m (about 1.59m below HTM) on day 1 to 0.19 (about 1.69m below HTM) by day 5. The visual profile shows that the plume enters the water table by about day 5 in this particular case. This may be caused by the infiltration from the flood tide which drives the plume down from the initial position (high conductivity zone) to a low conductivity region. The damping effects on the plume (difference in the movement of the plume at the high conductivity zone and at the low conductivity zone) at the top of the sediments would be therefore small in this case compared to greater depths. This characteristic behavior can be attributed to the mechanism of mass flux in the direction of the low conductivity region due to the net horizontal tidal flow, which induces level changes in the water table. As the shoreline moves inland and offshore with tidal level oscillations, the plume adapts to the pressure alteration above the capillary fringe in the unsaturated flow. Assuming the pressure at the beach face be constant, the temporal variations of the pressure gradient in the capillary fringe will mean that the zero-pressure location changes instantaneously. The pressure-gradient-induced water-table fluctuation is therefore responsible for the rate of advective spread of the injected dye in space. The orderly transformation of the plume describing the direction of mass transfer can thus be associated to the effect of fluctuations within the capillary zone. At varying levels of the instantaneous zero-pressure location during recharge, the capillary fringe approaches uniformity such that the local mass transfer (plume movement) rate is controlled by the low permeable materials with hardly visible water movement. In this particular scenario, the effect of the capillary fringe on mass transport may be small at the surficial region of the beach due to the high permeability. Also, the beach surface may experience low-frequency sea level oscillations with a corresponding response from the water table. However at greater depths (from about 1.5m below HTM), the effects of the capillary fringe become significant with low permeability as high-frequency sea level oscillations (tides) take over. This makes the plume front (bottom width) to spread less and become narrower (see Fig 9 (Top)). The effect of a receding tide on the injectate could be more significant than recharge, due to the slow expulsion of capillary water. Observations by Boufadel et al (2006) showed that tidal floods pushed the tracer mass vertically downwards along mean flow gradients while ebb-tides influenced spreading with the sea level oscillatory motion. The features in the frames (Fig 9 (Top)) demonstrate subsidence, movement and potential access of the contaminant into groundwater.

3.3.2 Scenario at OEIS-IZ (B) – summer

To give an objective interpretation of the complex scenarios here, the cases OEIS-IZ (B) were split into OEIS-IZ (B(i)) with subsidence similar to that observed in OEIS-IZ (A) and OEIS-IZ (B(ii)) lacking much subsidence. However, in OEIS-IZ (B(i)) cases the rate of subsidence and vertical spreading tends to decrease with depth, limiting the movement of the center of mass. In the case of OEIS-IZ (B(ii)), the resulting plume simultaneously diverges upwards and converges downwards. The results are unique and show that the surficial region of the sediments is prone to rapid rates of matter exchange, readily stimulating oxygen injection and utilization into deeper layers (Ehrenhauss and Huettel, 2004) as shown in Figs 9 (Top and Bottom). In Fig 9 (Bottom) the H_p relapses to 0.01m (about 1.51m below HTM) or 0.06m below surface after two complete tidal cycles (day 1). The plume further spreads upward to the surface water-sediment interface where the pressure is about constant, showing potential loss of contaminant to surface water from day 2 to day 5. The results show that the water tables at these two locations, namely OEIS-IZ (B(i)) and OEIS-IZ (B(ii)), are affected by the same tidal conditions but the plumes respond differently. Clearly the tidal oscillations and pressure fluctuations on the beach-sand are not uniform, hence the varying level of plume response. However, the pattern of spread (conically shaped plume) conforms to the inland-offshore oscillatory direction of net horizontal water movement.

This means that the effect of tides on the trapped contaminant (injectate) could also depend on the level and frequency of instantaneous water table fluctuation. The observation of the plume response in this area shows that the effects of sediment permeability and capillary pressure change are significant. Therefore, the effect of tidal water-level-induced BWT fluctuations on the trapped contaminant will depend on the permeability, magnitude and frequency of tidal oscillation over the beach. Furthermore, in addition to permeability, the topography of the beach face could influence the frequency of water table fluctuation in contrast to water movement in the subsurface. This observed behavior differing between OEIS-IZ (A) and OEIS-IZ (B) can be ascribed to the gravity development (Beinhorn et al, 2005) since the topography of the foreshore is not uniform. The plume widths shown in Fig 12 have potential implications for management decisions with respect to the surface and groundwater quality.

3.4 Analysis of spatial variability of plume

Fig 10 shows the average of plumes from Site-1 and Site-A of OEIS-IZ (A) which effectively relate to the movement described in Section 3.3. In other words, the response is such that as the low-frequency tide pushes the shoreline boundary inland, the high-frequency water table fluctuates. The movement of these two phases should therefore be responsible for the mass movement and capillary pressure effects (Li et al., 1997). For example, during the formation process (advective spreading of the plume), by the 2nd complete tidal-cycle the plume moves such that the center of mass moves down from the injection point (0.25,-0.05) to H (0.25,-0.169). After the 6th and 10th cycles the center moves further to I (0.25,-0.223) and N (0.25,-0.286) respectively while maintaining the full 2D-conical profile. This observation is consistent with Fig 10 where the first two tidal cycles also differ from the 10th. The center moves through point I (0.25,-0.1427) after 4 cycles to D_1 (0.25,-0.3375) after 10 cycles (all in meters). The negative sign indicates that the dye is below the beach sediment surface. The depths are subject to adjustment with respect to the HTM (about 1.50m above the beach surface at the injection region). Also from the samples averaged in OEIS-IZ (B), two distinct responses belonging to sites B(i) and B(ii) are observed. In site B(i), it was found that the full plume subsides (shifted downwards) like the previous case, but the fall-rate of the center of mass from the IP diminishes with increasing time . In site B(ii) [Fig 11] however, the plumes advect and spread while diverging upwards and converging downwards simultaneously. These characteristic observations could not have been driven by a singular environmental factor but by a combination of processes (tidal and water table fluctuations inducing pressure gradients on the foreshore, pore-fluid salinity, sediment properties). The combination here is unique and has not been reported in literature. For instance, the dye plumes reveal persistent vertical conical gradients, not spherical/elliptical shapes. It demonstrates unique and different transport of dye plume (pollutant) in tidal beach from transport in aquifers. The tidal impact on pollutant movement is different from contaminant transport in aquifers. The effect of each of these processes (tidal and water table fluctuations, etc. as above) on these observations could be further explored. The slowing translation of the center of mass in Fig 11 could be attributed to vertical mixing limiting kinetic energy due to interception from re-suspension flows. Moreover, since the beach acts as a filtrate and burial post, early minute deposits could consolidate deeper for new arrivals to continue the building process, hence, permeability differences could appear at the sample area. Furthermore, great average vertical cross-section of the plume is found in Fig 11, giving the impression of increased flow or mixing rates at the sediment grain-water interfaces at sites B. This could be due to the near-surface position of the center of mass, which is prone to rapid rates of matter exchange at the interface (Ehrenhauss and Huettel, 2004), since there is less or no evidence of subsidence at sites B.

The observations from Figs 10 - 11 clearly show that the dye plume varies strongly with time. The averaged plume patterns shown in Figs 10-11 also vary with location as described in the qualitative examples (see Fig 9). This implies that the tidal oscillations and pressure fluctuations on the beach-sand are also not uniform, and cause wider plume variability in space.

3.4.1 Analytic discussion of the advective spreading of plume features

Figs 12-13 demonstrate that the features of the plume vary considerably at each site but with a general tendency to spread. Fig 12 shows a description of mean data points of the bottom width W_2 for site 1, site A and site B. On average W_2 narrows spatially to between about 0.03 and 0.06m within the duration of the experiments in these beach sediments. The narrowing of W_2 is not sustained in space and time as shown in the distribution of data points. The similar concave trend in the curves suggests similarity of the beach characteristic properties. As the plume front penetrates deeper, the trend of spreading becomes highly variable, and dampens between the third and fourth days as suggested in the upward concave curves. The narrowing implies that permeability of these beach sediments decreases with depth. Also, in Fig 12, the Top width W_1 diverges with mean length varying between 0.06 and 0.11m. The larger values are associated with greater permeability and near-surface net horizontal water movement. Tidal oscillation causes the water table elevation to change or fluctuate instantaneously, which tends to enhance the mixing rates within the top sediment-water interface layer. The damping effect will be therefore limited by the high permeability of the surficial sediments as the shoreline water propagates inland or offshore. The contraction in the curves as downward concave in sites B(i) & B(ii) may not necessarily mean decreasing mixing rates at the near-surface but rather reduction in opaqueness of the dye due to loss. The observations clearly show higher horizontal mixing rates at the near-surface than that at greater depths, as shown in Fig 12. Fig 13 (a) shows the average depth of the top of the plume below the surface of the sediment (about 1.5m below HTM) at the sites under investigation. It is seen from Fig 13 (a) that the general trend of the averaged depth-to-surface data is related to a steady subsidence with time. The variations are consistent between all the sites with the exception of B(ii) which is associated with the examples of upward divergence observed in Fig 9. Shum (1995) acknowledged that the net horizontal wave driven oscillatory water movement induces sufficient fluxes over the ripple sand beach bed to initiate interfacial hydraulic flow. It can be seen here that at later times the top of the plume moved towards the near-surface sediment-water interface. This is an example of loss to surface water from buried point-sources as shown in Fig 9. The statistical averaged data from the sites shown in Fig 13(b) reveal that the vertical length of the plume varies between about 0.12 and 0.35m in space with time. The nonlinearity in the curves shows that the spreading slows and is even reversed at some later times. This is expressed in the downward-concave curves; from about day 3 or 4 the plumes tend to contract. This is caused by the vertical mixing limiting kinetic energy due to low permeability at more consolidated depths. However, plumes lengthen fast at sites B(ii) compared to the rest of sites. This may be due to continual upward and downward movement in response to the boundary condition changes at the beach face and sediment-water table interface. It is estimated that the mean depth of this segregated pore region is about Y = 1.724m below the HTM. Fig 13 (c) shows the averaged location of center of mass (Y_0) for sites 1, A & B. From the averaged analysis in Figs 10-11, Y_0 increases from 0.14 to 0.34m (about 1.64 – 1.84m below the HTM) at OEIS-IZ(A), from 0.13 to 0.29m at B(i) and 0.11 to 0.18m at B(ii). These values of Y_0 reflect the different patterns of contaminant mass transport observed at the two sites. This includes the fact that there is relative lack of subsidence in OIES-IZ (B(ii)). The observations are complex but the underlying interpretation may not deviate extensively from the basic understanding of induced internal waves or pressure variation generated through the rough permeable subsurface. In Fig 13 (d) the line represents the coefficient of variation (0.045 m/day) with time of the location of the center of mass Y_0 averaged from all the sites. The coefficient of variation shows that after injection the centre of the plume moves down from about 0.09m to 0.315m (about 1.6m – 1.82m below the HTM) by the end of the fifth day. Increased uncertainty in the centre of mass location with time could influence the quantification of the contaminant distribution. However, the center-line (linear model) is a good statistical indicator of the outcome.

The observations in this field study mostly agree with the findings from related studies. For instance, Horn (2002) showed that tidal current modulation and water table pumping were characteristic factors affecting contaminants in beach sediments exposed to strong tides. While these factors distribute tidal energy through relatively large space, they are also able to cause the migration of dye in the beach subsurface. Boufadel et al (2006) observed that flood-tides draw the tracer mass down vertically along mean flow gradients whereas ebb-tides influence them to spread in-tune with the oscillatory motions. The divergence and convergence of W_1 and W_2 respectively are in agreement with observations in literature. Webster (1992) and Williams et al (2003) concluded in their observations that advective dispersion may control transport at the surficial pore regions of sediments while shear dispersion dominates at deeper levels due to sustained tidal and wave currents. It is expected that more of the dye will be lost to surface water at OEIS-IZ (B) than at OEIS-IZ (A) where the tracer predominantly moved downwards and may subsequently enter the groundwater aquifer. Reimers et al (2004) found the mean downward flow to decrease downwards.

4 UNCERTAINTY CHARACTERISATION

The spatial variability of the dye was monitored over time and sampled to investigate the transformation at the source. The resulting plume was then manually measured in the field. Errors in this quantification process could result in uncertainties due to several factors. For example, it was not possible to visualize and measure instantaneously, the variables determining the transitional stages and differences in the behaviour of the dye at the OEIS-IZ (A) and OEIS-IZ (B). The potential sources of uncertainty in this case therefore may be greater than in surface-water transport experiments. However, our method enables direct visualization of the advectively-spreading plume associated with the movement of the dye in the subsurface. Three sources of uncertainty that could be associated with the data quantification process therefore could be: (1) uncertainty in data collection due to measurement error and bias; (2) variability of measured parameters, arising from the investigators' view and method of assessment of 'opaqueness' of the spread plume; and (3) measurement errors leading to uncertainty of parameter estimation, such as incomplete sampling (e.g., limited knowledge of the beach sand properties) and uncertain boundary conditions.

The aforementioned uncertainty sources in this study therefore could be attributed to high variability of soil compaction and pore-size distribution. Additionally, the events monitored occurred under periodic interchanges between saturated and unsaturated beach material (intertidal). This implies that the hydraulic conductivity will also vary with position within the subsurface granular regions. Soil-water tension or moisture content when unsaturated is important information for uncertainty reduction in dye displacement. The measurement of the travel path described in our conical plume formation therefore is informative and an important factor towards reducing uncertainty of displacement rates in coastal subsurface materials.

5 SUMMARY AND CONCLUSION

We investigate the spatial variability of contaminants in a coastal intertidal sand beach using results from field experiments. The experiments involve injection of tracer dye into the top soil at five different sites, and geotechnical study. After the completion of each session of injection, the spatial variability of the evolving plume in the field is monitored over time, sampled at the source and manually measured. The process is repeated up to seven consecutive days over a period of four summer months in two years and the transport of the tracer plume analyzed to quantify the injectate advective distribution. The procedure centres on the beach-sand vadose zone of the coastal foreshore in contrast to contaminant transport in groundwater aquifer studies. In addition, the method differs from previous studies where the injection position of the dye (source point) was different from the monitoring point.

The evolved range of dye plumes found here has not been reported in literature. Based on the features analyzed, the plumes show persistent vertical conical gradients instead of the widely known spherical/elliptical shapes. The features analyzed can be utilized to evaluate flow rates (pore velocity), dispersion, and concentration data with a view to determine groundwater flow paths and contaminants' fates in intertidal coastal beach sediments. The visual accounts of the temporal and spatial variations of the plume are presented with satisfactory evidence of the response mechanism in the subsurface. The vertical profiles of plume cross-section can be related to local influence of flow ponding and low hydraulic conductivity zones with localized and dense accumulation stages. The sampled temporal and spatial plume data are insightful, and can inform relevant future numerical studies and practice-based research.

Results from this field study at the RME suggest that dye discharges into watercourses can actually enter coastal beach sediments through diffusive fluxes due to tides. The fluxes according to the study can also drive beach-sediment-applied-dye to resurface in seawater courses and also enter groundwater courses. A recent example is the 2010 widely publicized Gulf of Mexico oil accident where crude oil was found deep in beach sediment. Similar scenarios have also been reported in the crude-oil-rich Niger Delta regions of Nigeria where oil leaks due to rupture from submerged pipelines enter surface and groundwater courses, causing serious catchment concerns. This is also in agreement with findings by Boudreau et al (2001) and Boufadel et al (2006) that the surficial inland - offshore tides can induce large fluxes exceeding interstitial diffusive flux in the beach vadose zone. The ability therefore to visualize naturally induced advective transport of contaminant dye at the sediment-water interface can be a robust means of assessing fate through groundwater tracing techniques.

It is expected that this study will provide the unique benchmark dataset for numerical modelers to validate their models, which in turn could be used to extend the current field study in terms of including broad ranges of key parameters.

Acknowledgement: The research reported in this paper is financially supported by China Ministry of Science and Technology 973 program (2014CB745001), Special Program of future development in Shenzhen (201411201645511650) and Shenzhen Key Laboratory for Coastal Ocean Dynamic and Environment (ZDSY20130402163735964). The constructive comments and suggestions made by the Associate Editor and four anonymous Reviewers have greatly improved and enhanced the quality of the paper.

REFERENCES

Admiralty (2005). *Admiralty Tide Tables*. Volume 1, 2006. Admiralty Charts and Publications, Chart NP201. United Kingdom Hydrographic Office, Taunton.

Arch, J. Stephenson, E. and Maltman, A. (1993). Factors Affecting the Containment Properties of Natural Clays, Proc. Conf. the Engineering Geology of Waste Disposal and Storage, Cardiff, pp 263-272.

Ataie-Ashtiani, B., Volker, R. E. and Lockington, D. A. (2001). Tidal effects on groundwater dynamics in unconfined aquifers. *Hydrological Processes*, **15**, 655–669.

Ataie-Ashtiani, B., Volker, R.E., Lockington, D.A., (1999). Tidal effects on sea water intrusion in un- confined aquifers. *Journal of Hydrology* 216, 17-31.

Baird, A. J., Horn, D. P. 1996. Monitoring and modelling groundwater behaviour in sandy beaches. *Journal of Coastal Research* 12(3): 630–640.

Banin, A. and D.M. Anderson (1974) Effects of salt concentration changes during freezing on the unfrozen water content of porous materials. *Water Resources Research*, 10: 124–128.

Beinhorn, M., Dietrich, P., Kolditz, O. 2005. 3-D numerical evaluation of density effects on tracer tests. *Journal of Contaminant Hydrology* 81(1-4): 89-105.

Berkowitz, B., Dror, I., Yaron, B. 2008. Contaminant Geochemistry: Interactions and Transport in the Subsurface Environment. Springer-Verlag Berlin Heidelberg.

Blott, S. J. and Pye, K. (2001). Gradistat: A grain size distribution and statistics package for the analysis of unconsolidated sediments. *Earth Surface Processes and Landforms* **26**, 1237–1248.

Boufadel, M. C., Suidan, M. T. and Venosa, A. D. (2006) Tracer Studies in Laboratory Beach Simulating Tidal Influences. *Journal of Environmental Engineering*, 6 (132).

Butler, J.J. (1998). *The Design, Performance, and Analysis of Slug Tests*, New York: Lewis

Publishers.

Böer S. I., Arnosti, C., van Beusekom, J. E. E. and Boetius, A. (2009). Temporal variations in microbial activities and carbon turnover in subtidal sandy sediments. *Bio- geosciences*, 6, 1149–1165.

Carrier, W.D. 2003. Goodbye, Hazen; Hello, Kozeny-Carman. Journal of Geotechnical and Geoenvironmental Engineering.1054.

Christodoulou & A. I. Stamou (eds). CRC Press, Taylor & Francis Group, Lon- don, ISBN 978-0-415-58475-3.

de Marsily, G., (1986). *Quantitative Hydrogeology: Groundwater Hydrology for Engineers*, Academic Press, N.Y.

Denham, M. and Vangelas, K. M. (2008). Biogeochemical gradients as a framework for un-derstanding waste-site evolution. *Remediation*, 19 (1), 5-17.

Diaw, E. B., Lehmann, F., Ackerer, Ph. 2001. One-dimensional simulation of solute transfer in saturated–unsaturated porous media using the discontinuous finite elements method. *Journal of Contaminant Hydrology* 51(3-4): 197-213.

Environment Agency, (2001). The distribution of organotin compounds in water and sediments in Liverpool Bay and the Mersey Estuary. *Environment Agency*, reMSP-01-07.

Fetter, C. W. (1999). *Contaminant Hydrogeology*. Second Edition, Prentice Hall Upper Saddle River, NJ 07458.

Fischer, H. B., List, E. J., Koh, R. C. Y., Imberger, J., Norman, H. B., (1979). *Mixing in inland coastal waters*. Academic Press, London.

Ford, D. and Williams, P. (1989). Karst Geomorphology and Hydrology, Unwin Hyman Ltd, London.

Fox, W. M., Johnson, M. S., Jones, S. R., Leah, R. T., Copplestone, D. (1999). The use of sediment cores from stable and developing salt marshes to reconstruct historical contamination profiles in the Mersey Estuary, UK. *Marine Environmental Research*, 47, 311-329.

Freeze, R. A. and Cherry, J.A. (1979). *Groundwater*. Prentice-Hall, Inc., N. J.

Gray, D.M. and R.J. Granger (1986) In situ measurements of moisture and salt movement in freezing soils. *Canadian Journal of Earth Science*, 23: 696–704.

Horn, D.P. (2002). Beach groundwater dynamics. *Geomorphology* 48, 121–146.

Huang, W.E., C.C. Smith, D.N. Lerner, S.F. Thornton, A. Oram. (2002). Physical modelling of solute transport in porous media: evaluation of an imaging technique using UV ex- cited fluorescent dye. *Water Research,* 36: 1843–1853.

Huettel, M., Ziebis, W. and Forster, S. (1996). Flow induced uptake of particulate matter in permeable sea beds. *Limnology and Oceanography* 41: 309-322.

Itugha, O. D. (2008). Solute and particulate transport at the interface of near-shore permeable estuarine beach-sand: an experimental study of the outer reaches of River Mersey estuary, N W England. Harold Cohen; THESIS 20860.ITU, Liverpool: Thesis Ph.D., 2008

Itugha, O. D., Chen, D. and A.A. Ahmed (2010). Solute migration and transport in coastal sand-beach sediments under strong tides. Vol. 2, 935-940. *In* Environmental Hydraulics – G. C.

Jones, P. D., (2006). Water quality and fisheries in the Mersey estuary, England: A historical perspective. *Marine Pollution Bulletin* 53: 144–154.

Kalbus, E., Reinstorf, F., and Schirmer, M. (2006). Hydrology and Earth System Sciences, 10, 873–887, 2006

Khalili A, Basu AJ, Pietrzyk, U. (1998). Flow visualization in porous media via Positron Emission Tomography. *Physics of Fluids*, 10:1031–3.

King, A.J., Readman J.W. and Zhou J.L. (2004). Determination of polycyclic aromatic hydro-carbons in water by solid-phase microextraction - gas chromatography - mass spectrometry. *Analytica Chimica Acta* 523(2): 259-267.

Klute, A., Dirksen, C. (1986). Hydraulic conductivity and diffusivity: laboratory methods. In: Klute, A. (Ed.), Methods of Soil Analysis. Part 1. Physical and Mineralogical Methods, 2nd ed. Agron. Monogr. 9. ASA, Madison, WI, pp. 687–734.

Lanyon, J. A., Eliot, I. G. Clarke, D. J. (1982). Groundwater–level variation during semidiurnal spring tidal cycles on a sandy beach. *Aust. J. Mar. Freshwater Res.* 33: 377-400.

Li, H., Sun, P. Chen, S., Xia, Y. and Liu, S. (2009). A Falling-Head Method for Measuring Intertidal Sediment Hydraulic Conductivity. *Ground Water,* doi: 10.1111/j.1745-6584.2009.00638.x

Li, L., Barry, D.A., Pattiaratchi, C.B. (1997). Numerical modelling of tide-induced beach water table fluctuations. *Coastal Engineering* 30, 105–123.

Li, Y., Ghodrati, M. (1995). Transport of nitrates in soils as affected by earthworm activities. *Journal Environmental Quality* 24: 432-438.

Mao, X., Enot, P., Barry, D.A., Li, L., Binley, A., Jeng, D.-S. (2006) Tidal influence on behaviour of a coastal aquifer adjacent to a low-relief estuary. *Journal of Hydrology*, 110–127.

McNeil, J. D., Oldenborger, G. A., and Schincariol, R. A. (2006). Quantitative imaging of contaminant distributions in heterogeneous porous media laboratory experiments. *Journal of Contaminant Hydrology* 84: 36–54.

Nakano, Y. (1995). *Transport of Tracer Br in Frozen Morin Clay in Response to Temperature Gradients*. Cold Regions Research & Engineering Laboratory (CRREL) Report 95-3. US Army Corps of Engineers.

Nielsen, P. (1999). Groundwater Dynamics and Salinity in Coastal Barriers. *Journal of Coastal Research*, 15(3), 732-740.

Nielsen, P., 1990. Tidal dynamics of the water table in beaches. *Water Resources Research* 26: 2127-2134.

Peck, L. (1998). *Remediation of Wastewater by Land Treatment Consideration of Soil Temperatures in Winter*. Cold Regions Research & Engineering Laboratory (CRREL) Report 98-8. US Army Corps of Engineers.

Philip, J. R. 1973. Periodic non-linear diffusion: an integral relation and its physical consequences. *Australian Journal of Physics* 26: 513–519.

Precht, E., Huettel, M. (2004). Rapid wave-driven advective pore water exchange in a permeable coastal sediment. *Journal of Sea Research,* Vol. 51, pp. 93–107.

Reimers, C. E., Stecher III, H. A., Taghon, G. L., Fuller, C. M., Huettel, M., Rusch, A., Ryckelynck, N., Wild, C. 2004. In situ measurements of advective solute transport in permeable shelf sands. *Continental Shelf Research* 24 (2004) 183–201.

Robbins, G. A. 1989. Methods for determining transverse dispersion coefficients of porous-media in laboratory column experiments. *Water Resource Research* 25:1249–1258.

Rogers, H. R. (2002). Assessment of PAH contamination in estuarine sediments using the equilibrium partitioning–toxic unit approach. *Science of the Total Environment* 290:139–55.

Schincariol, R.A., Herderick, E.E., Schwartz, F.W. (1993). On the application of image analysis to determine concentration distributions in lab expts. *J. of Contaminant Hydrol.* 12: 197-215.

Schirmer, M., Molson, J.W., Frind, E.O., Barker, J.F. (2000). Biodegradation modelling of a dissolved gasoline plume applying independent laboratory and field parameters. *Journal Contaminant Hydrology*, 46 (3–4), 339–374.

Shum, K. T. and Sundby, B. (1996) Organic matter processing in continental shelf sediments - the subtidal pump revisited. *Marine Chemistry*. 53:81-87.

Sundby, B. (2001). Permeable marine sediments: Overturning an old paradigm. *EOS Transcripts Am. Geophysics,* 82, 135-136.

Swartz, C. H. and Schwartz, F. W. (1998): An experimental study of mixing and instability development in variable-density systems, *Journal of Contaminant Hydrology* 34: 169–189.

Todd, D. K. (1980). *Groundwater hydrology*, 2nd edition. Wiley, New York.

Turner, I. L., and Nielsen, P., (1997). Rapid Water Table Fluctuations within the Beach Face : Implications for Swash Zone Sediment Mobility. Coastal Engineering , 37, 45-59.

Turner, I. L., Coates, B. P. and Acworth, R. I. (1996). The Effects of Tides and Waves on Water-Table Elevations In Coastal Zones. *Hydrogeology Journal* 4(2): 51-69.

Vane, C.H. I. Harrison, A.W. Kim (2007). Polycyclic aromatic hydrocarbons (PAHs) and polychlorinated biphenyls (PCBs) in sediments from the Mersey Estuary, U.K. *Science of the Total Environment,* 374, 112–126.

Webster, I. T., and Taylor, J. H., (1992). Rotational dispersion in porous media due to fluctuating flows. *Water Resources Research* 28: 109-119.

Weight, W. D., Sonderegger, J. L. (2001). *Manual of Applied Field Hydrogeology*. McGraw-Hill Companies, Inc., USA.

Wexler, E. J. (1992). *Analytical solutions for one-, two-, and three dimensional solute transport in groundwater systems with uniform flow*. USGS-TWRI Book 3, Chap B7.

Wilson, A. M. and Gardner, L. R. (2006). Tidally driven groundwater flow and solute exchange in a marsh: Numerical simulations. *Water Resources Research*, Vol. 42, W01405.

Woodworth, P.L., Tsimplis, M.N., Flather, R.A., Shennan, I., (1999). A review of the trends observed in British Isles mean sea level data measured by tide gauges. *Geophysical Journal International* 136 (3), 651-670.

Woodworth, P. L. and Blackman, D. L. (2002). Changes in Extreme High Waters At Liverpool Since 1768. *International Journal of Climatology* 22: 697–714 (2002).

WPRL (1974). Effect of Polluting Discharges on the Mersey Estuary. Report of Investigations on behalf of the Steering Committee on Pollution of the Mersey Estuary. WPRL Report 447R.

Zhang, Q.; Volker, R. E.; Lockington, D. A. (2002). Experimental investigation of contaminant transport in coastal groundwater. *Advances in Environ. Res.* 6: 229-237.

Fig 1: Area map with markers showing the injection zones and Marine Lake at the sheltered boundary of the outer RME with overview map (*at the right shows the RME*).

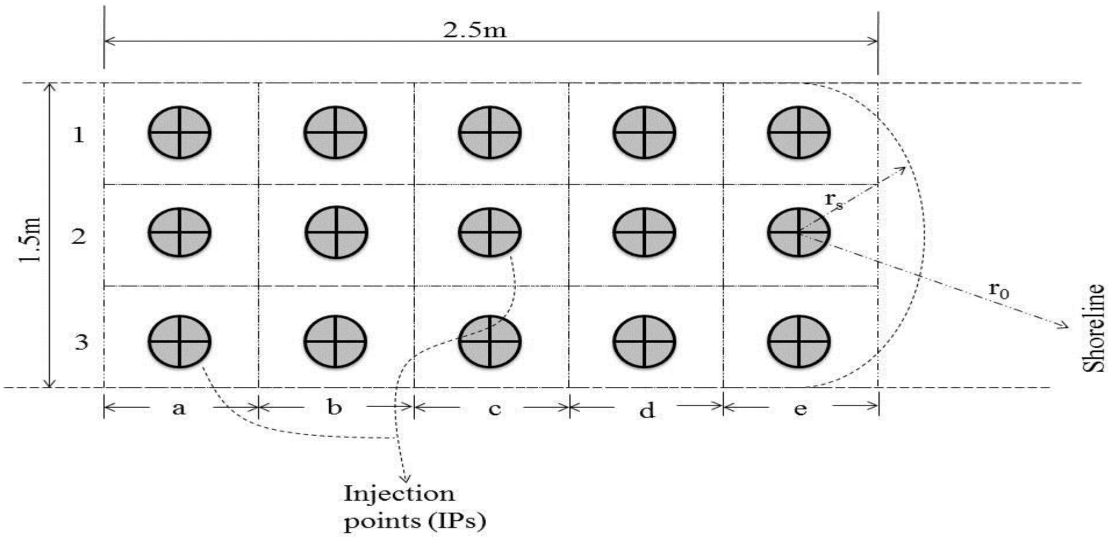

Fig 2: Arrangement of rectangular cross-section of IPs in a typical field site with column/row divisions (*columns are represented by a, b, c, …, and rows by 1, 2 & 3 such that a_1, a_2,…represent IPs in the 1st column, etc.; r_s = radial distance at a point from an IP; r_0 = radius of influence, a function of the shoreline distance and permeability*.)

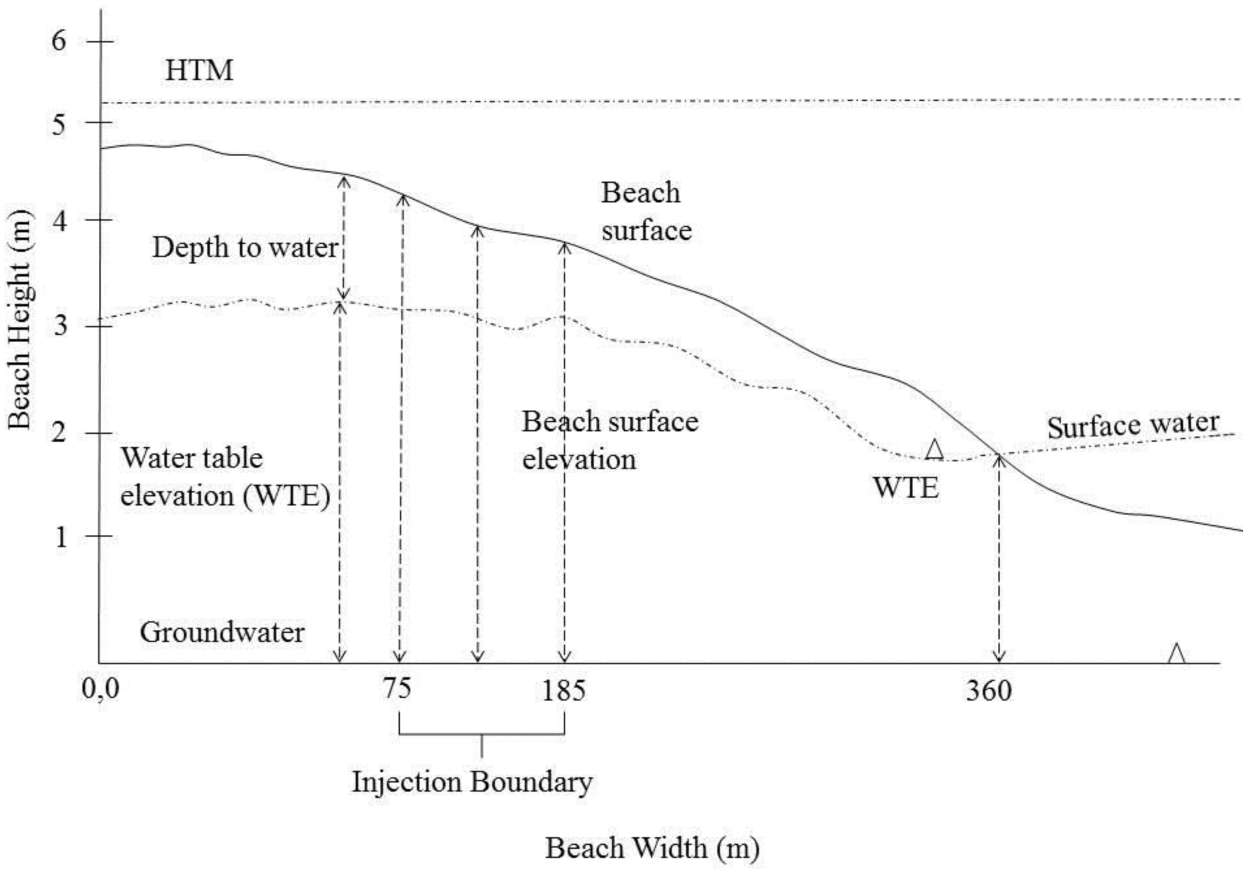

Fig 3: Sketch illustrating the intertidal (shoreline - inland bank) divisions with water table elevation (WTE), injection area and tidal water marks at the RME [*high tide mark (HTM))*]

Table 1: Summary of field experiment during the summer (April-July 2006; 2007)

Experimental Area	Injection Zone	Number of IP locations @		Total IPs @		Total IPs mined @	
		3*5 array	5*5 array	3*5 array	5*5 array	3*5 array	5*5 array
N56 26 W03 02	OEIS-IZ (A)	57	4	855	100	513	65
N56 26 W03 03	OEIS-IZ (B)	32	2	480	50	264	30
	OEIS-IZ (C)	7	1	105	25	63	10
N56 26 W03 02	NEIS-IZ (A)	16	2	240	50	99	35
	NEIS-IZ (B)	6	1	90	25	27	10
Total				**1770**	250	**966**	150

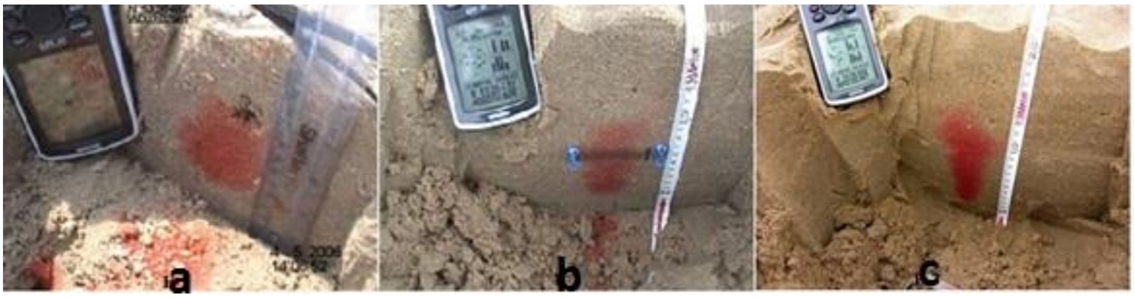

Fig 4: (a) about 4-5 hours after injection (no flood case), (b) after one complete tidal cycle and (c) two complete tidal cycles.

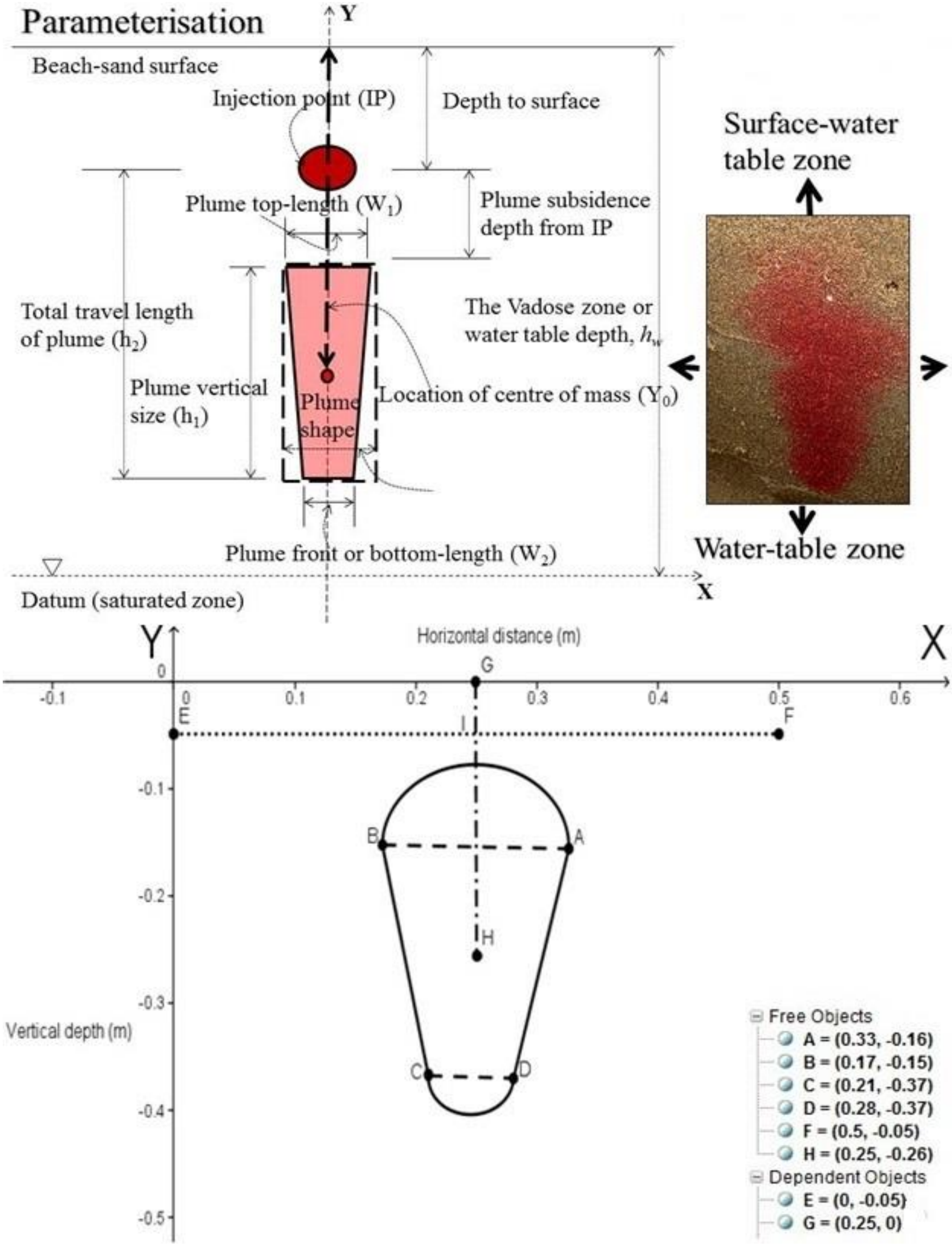

Fig 5: The upper part illustrates the parameter of the plume and direction of movement in space and the lower graph shows analysis of the plume with coordinates using a trapezoidal identity. [*BA = W_1, CD = W_2, EF = 0.5m length of square cell, GI = depth to surface, GH = location of centre of mass*]

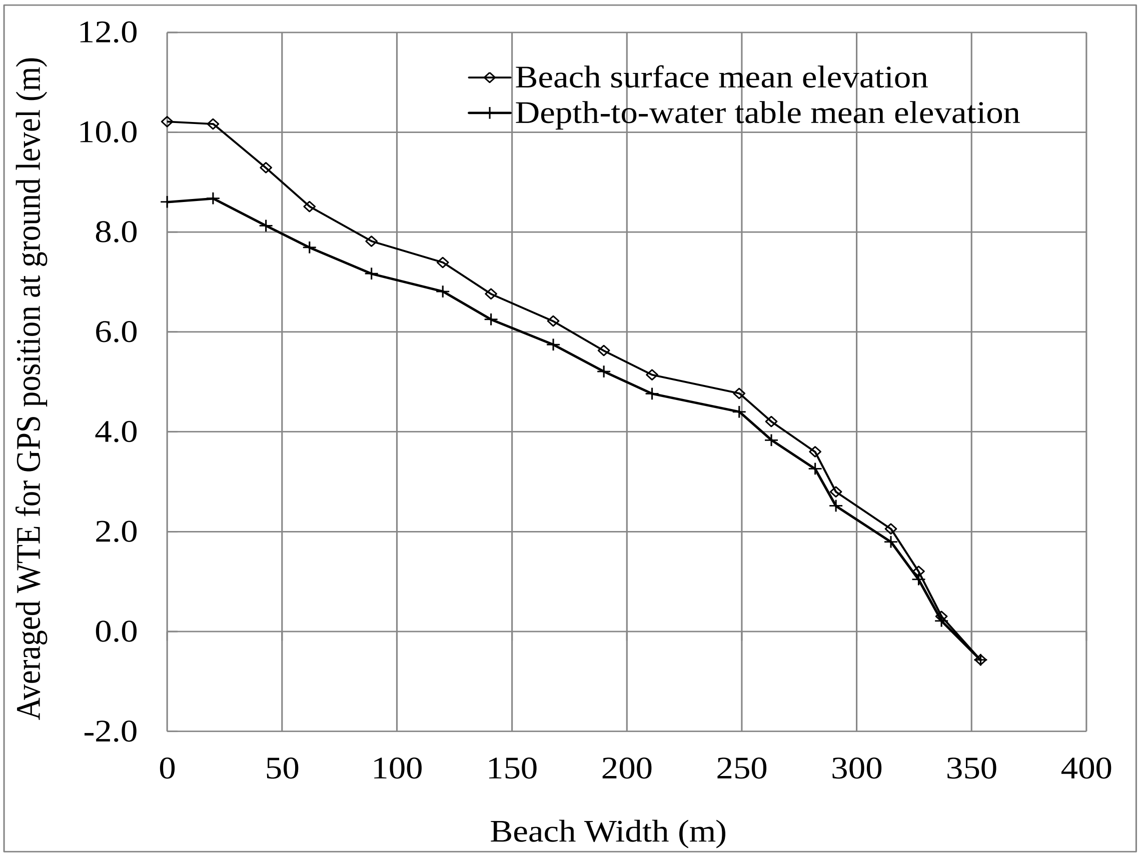

Fig 6: Water table elevation relative to the beach surface elevation at the OEIS-IZ (A)

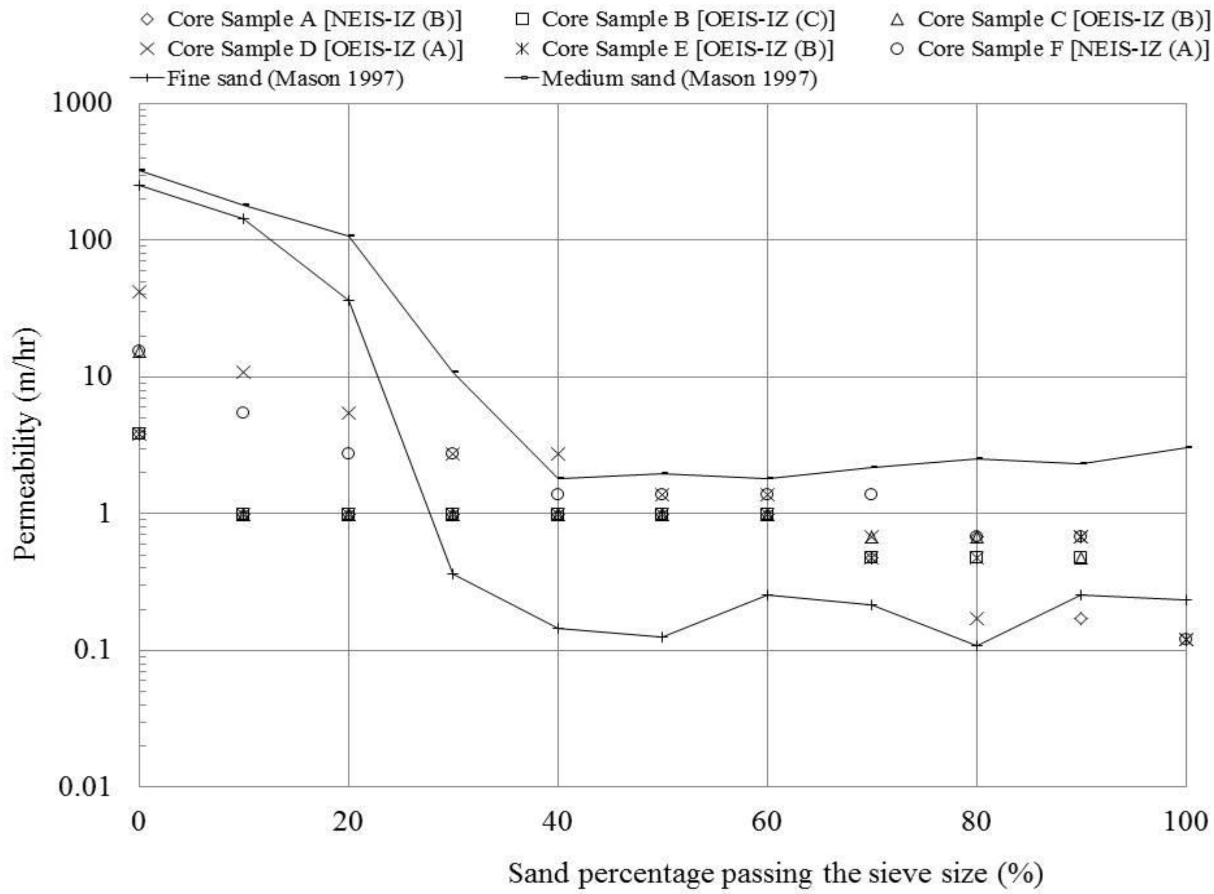

Fig 7: Permeability of core samples taken from injection sites showing grain-size differences using the Kozeny-Carman relation.

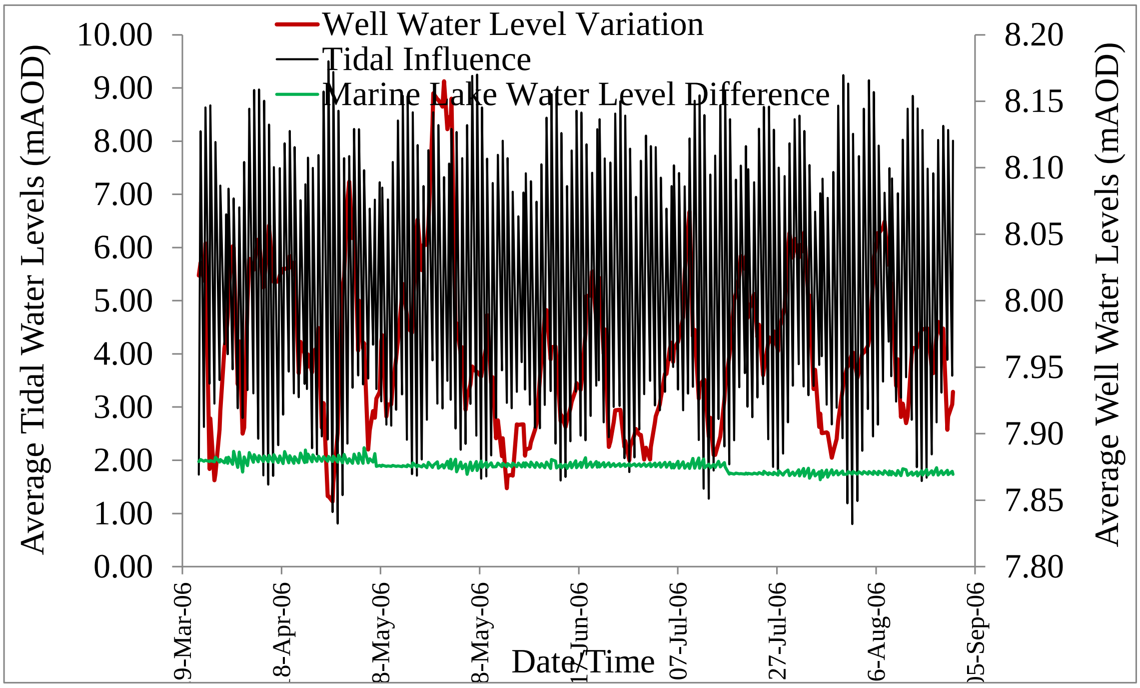

Fig 8: Correlation of SWL and groundwater level changes at the sheltered coast

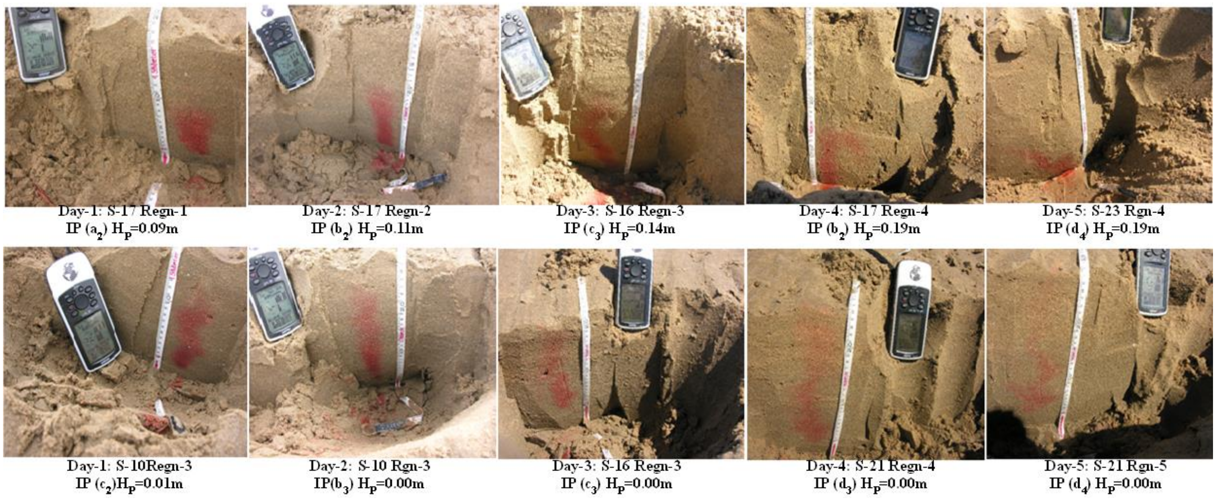

Fig 9: Plume subsidence from high conductivity (permeability) into low conductivity depth as observed in-situ at OEIS-IZ(**A)** – Top; Plume spread in low & high conductivity zones as observed in-situ at OEIS-IZ (B) – Bottom. [*site (S), Regn (region), IP (injection point), 5ml/5cm (solute amount injected is 5ml and injection depth is 5cm), H_p (height of plume-top below injection-depth)]*

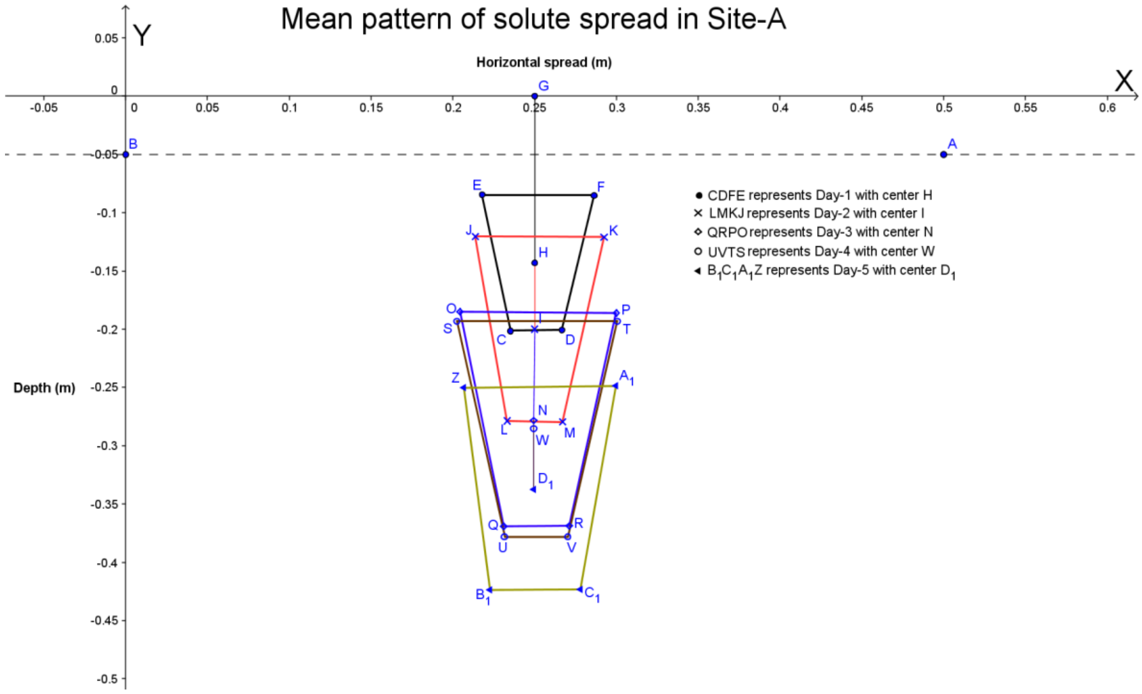

Fig 10: Averaged features of conical plume at Site-A [OEIS-IZ (A)] for day 1; day 2; day 3; day 4; day 5

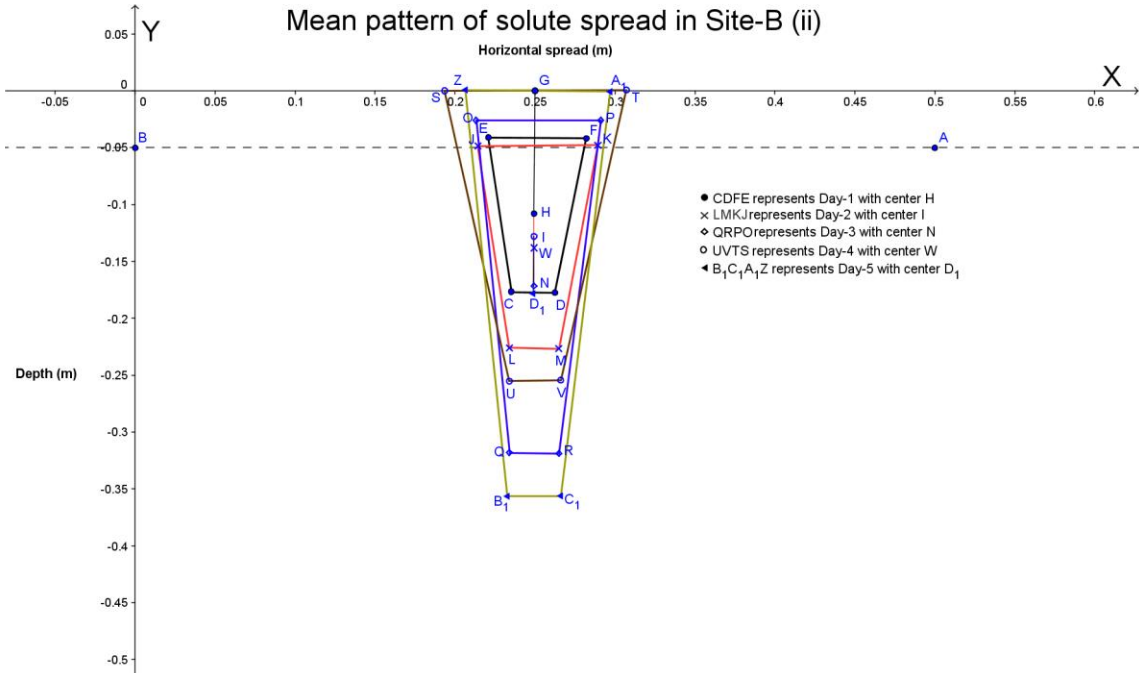

Fig 11: Averaged features of conical plume yield with depth in Sites B(ii) [OEIS-IZ (B)] for day 1; day 2; day 3; day 4; day 5

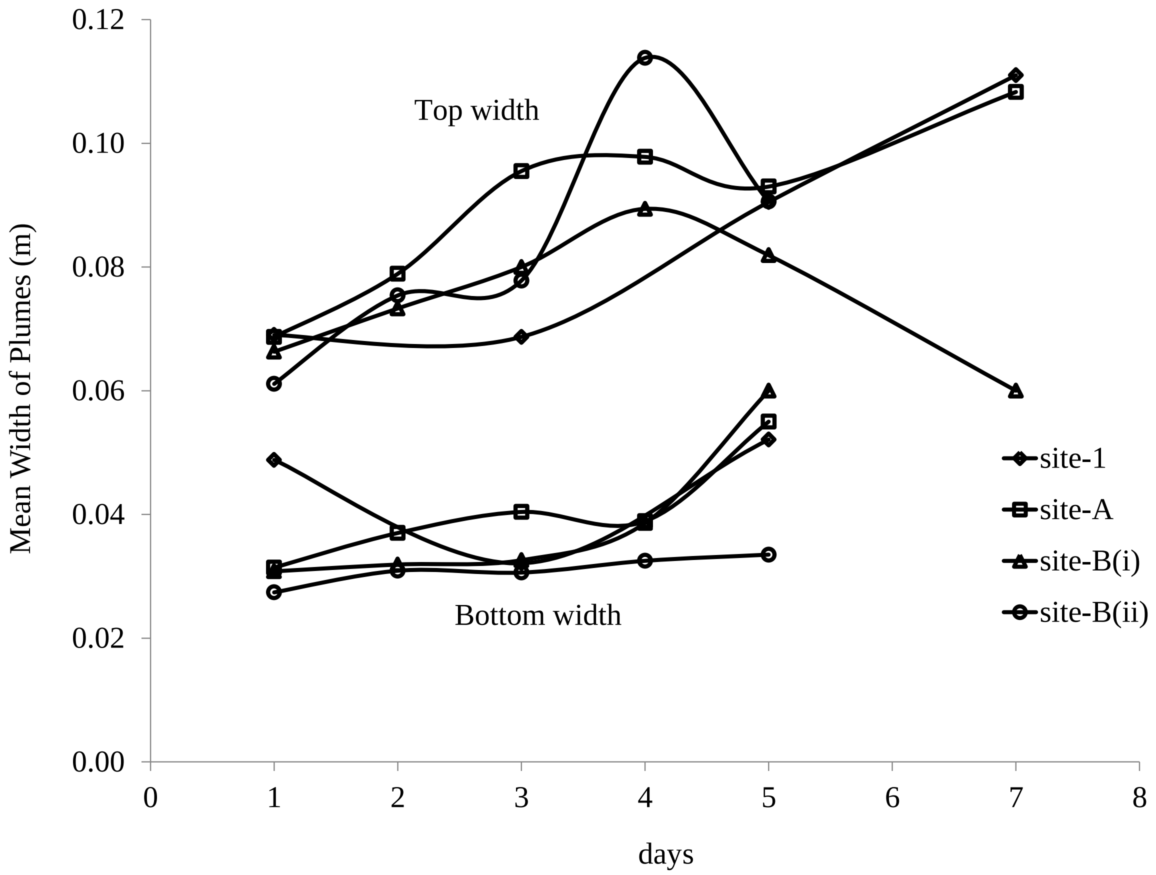

Fig 12: Comparisons of the variations of mean top widths and bottom widths of plumes in Sites (1, A & B)

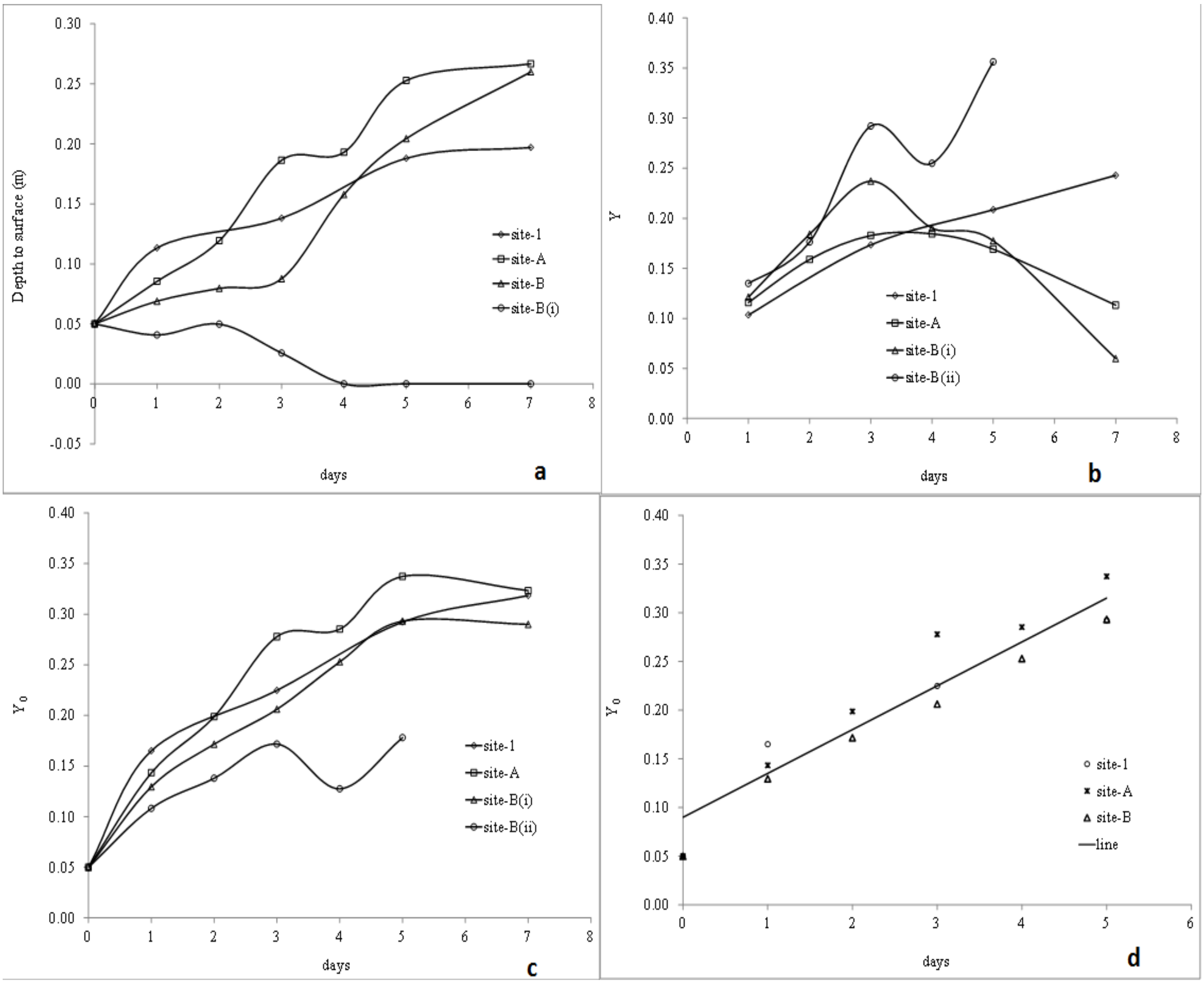

Fig 13: Comparisons in Sites 1, A & B: (a) Mean variation of plumes in space away from the beach-sand surface with time. (b) Mean vertical length of plumes. (c) Mean depth of plume center of mass to surface. (d) Linear model with regression line for deepening center of mass.